Evaluation of Iodine-125 Interstitial Brachytherapy Using Micro-Positron Emission Tomography/Computed Tomography with 18F-Fluorodeoxyglucose in Hepatocellular Carcinoma HepG2 Xenografts

Authors' Contribution:
Study Design A
Data Collection B
Statistical Analysis C
Data Interpretation D
Manuscript Preparation E
Literature Search F
Funds Collection G

ABF 1 **Yangjun Zhu**
DF 2 **Mengjie Dong**
BE 2 **Jun Yang**
CE 2 **Jun Zhang**

1 Department of Ultrasonography, The First Affiliated Hospital, College of Medicine, Zhejiang University, Hangzhou, Zhejiang, P.R. China
2 Department of Nuclear Medicine, The First Affiliated Hospital, College of Medicine, Zhejiang University, Hangzhou, Zhejiang, P.R. China

Background: Iodine-125 interstitial brachytherapy (^{125}I-IBT) is a promising treatment option for unresectable hepatocellular carcinoma (HCC). This study evaluated the usefulness of micro-positron emission tomography/computed tomography (micro-PET/CT) with ^{18}F-fluorodeoxyglucose (^{18}F-FDG) in assessing response to ^{125}I-IBT in HCC HepG2 xenograft.

Material/Methods: Twelve mice with bilateral HepG2 xenografts were divided into 3 equal groups implanted with iodine-125 seeds into the left xenografts with a dose of 30, 50, and 80 Gy, respectively, and the right xenografts were used as internal controls. Before and 28 days after treatment, the ^{18}F-FDG micro-PET/CT was performed. The ratios of left to right xenografts of tumor volume (R_{TV}), maximum standardized uptake value (R_{SUVmax}), mean optical density of caspase-3 expression ($R_{MODcaspase-3}$), and apoptosis index (R_{AI}) were compared.

Results: The R_{TV} means of the 50 and 80 Gy groups were significantly lower than in the 30 Gy group after treatment ($P<0.01$) and the R_{TV} means after treatment were lower than baseline in the 50 and 80 Gy groups ($P<0.05$). The R_{SUVmax} mean after treatment was lower than baseline in the 80 Gy group ($P<0.05$). The $R_{MODcaspase-3}$ and R_{AI} means of the 80 Gy group were higher than in the 30 Gy group ($P<0.05$). The R_{SUVmax} was correlated negatively to $R_{MODcaspase-3}$ ($r=-0.624$, $P<0.05$) and R_{AI} ($r=-0.651$, $P<0.05$).

Conclusions: This study suggest that ^{125}I-IBT inhibits tumor growth via upregulating caspase-3 expression and prompting apoptosis in HCC HepG2 xenografts. The ^{18}F-FDG micro-PET/CT may be a useful functional imaging modality to assess early response to ^{125}I-IBT in HCC HepG2 xenograft.

MeSH Keywords: Brachytherapy • Carcinoma, Hepatocellular • Fluorodeoxyglucose F18 • Positron-Emission Tomography • X-Ray Microtomography

Full-text PDF: https://www.medscimonit.com/abstract/index/idArt/912590

📄 2890   ▥ 4   📊 4   📖 51

Background

Liver cancer is the one of the most common malignancy worldwide, with nearly 800 000 new cases and 745 500 deaths in 2012. Hepatocellular carcinoma (HCC) accounts for about 70–90% of primary liver cancer [1]. HCC usually has a poor prognosis due to being diagnosed frequently at advanced stage or with underlying liver dysfunction [2–5]. Moreover, it tends to invade vasculature and then forms a tumor thrombus, leading to a worse prognosis [6]. At present, although many treatments are available, the 5-year relative survival rate is only 18% for all stages of HCC [7]. Surgical resection, liver transplantation, and ablation offer a high complete response rate and, thus, potential for cure. Transarterial chemoembolization (TACE) and sorafenib are the only non-curative treatments that improve survival. Arterial embolization without chemotherapy, external radiotherapy, and radioembolization have shown antitumor activity, but no survival benefit has been proven [8]. Recently, iodine-125 interstitial brachytherapy (125I-IBT) has been employed as a promising approach for the treatment of unresectable HCC and tumor thrombus, alone or in combination with other therapy [9–16]. It has the advantages of maximizing radiation dose within the tumor to kill tumor cells and minimizing radiation injury of surrounding normal liver tissue.

Treatment response is mainly evaluated based on tumor dimension measurement using anatomic modalities such as ultrasonography, computed tomography (CT), and magnetic resonance imaging, but it is not informative, as necrosis may not be paralleled by tumor burden reduction [17]. Positron emission tomography/CT (PET/CT) using ^{18}F-fluorodeoxyglucose (^{18}F-FDG), which is a kind of anatomic and functional fusion imaging reflecting glucose metabolism in tumor cells based on Warburg effect, has emerged as a powerful tool for initial diagnosis and staging, detecting recurrence and metastasis, and monitoring response to chemotherapy and/or radiotherapy in malignancies [18–22]. In the present study, the usefulness of ^{18}F-FDG micro-PET/CT in assessing response to ^{125}I-IBT with different radiation doses was evaluated in HCC HepG2 xenografts.

Material and Methods

Cell culture and animal model

The human liver cancer cell line HepG2 was obtained from the Shanghai Cell Bank (Shanghai, China). RPMI-1640 medium, fetal bovine serum (FBS), streptomycin, and penicillin were purchased from Gibco, Thermo Fisher Scientific, Inc. (Waltham, MA, USA). HepG2 cells were grown in RPMI-1640 medium supplemented with 10% (v/v) FBS, 100 µg/ml streptomycin, and 100 U/ml penicillin. Cells were incubated at 37°C in a humidified atmosphere containing 5% CO_2, and trypsinized

and harvested after reaching 70–80% confluence. Male BALB/c-nu mice (18–20 g, 4–6 weeks old) were purchased from Shanghai SLAC Laboratory Animal Co. (Shanghai, China) and allowed to acclimatize for 1 week in a specific pathogen-free room under controlled temperature and humidity before experiments began. Following this, ~0.1 ml HepG2 cell suspension (1×10^{7} cells/1 ml RPMI-1640) was injected subcutaneously into the bilateral armpits of forelegs. After 4 weeks, mice with a xenograft diameter of ~10 mm were used for the study. The animals used in this study received humane care in compliance with the Guidelines for the Care and Use of Experimental Animals established by the Medical Ethics Committee on Animal Experiments of Zhejiang University.

Study design

A total of 12 mice were randomly divided into 3 groups (n=4 per group): a 30-Gy group implanted with an ^{125}I seed with mean activity of 0.36 mCi, a 50-Gy group implanted an ^{125}I seed with mean activity of 0.62 mCi, and an 80-Gy group implanted with 2 ^{125}I seeds with mean activity of 0.50 mCi into the left xenografts on mice, while the right xenografts were used as internal controls. The treatment period was 4 weeks. Tumor growth was monitored by determining the xenograft size every 2 days with a calliper. Before and 28 days after ^{125}I-IBT, micro-PET/CT imaging was performed to determine the baseline level and post-treatment alterations in ^{18}F-FDG uptake. At the end of the study, the mice were euthanized by dislocation of cervical vertebra after being anesthetized with 3% isoflurane inhalation, and all xenografts were histologically analyzed with immunohistochemical (IHC) and terminal- deoxynucleotidyl transferase mediated nick-end labeling (TUNEL) staining.

Interstitial brachytherapy and tumor volume

The ^{125}I seeds (Model 6711 with a diameter of 0.8 mm, length of 4.5 mm, half-life of 59.6 d, half-value thickness of 1.7 cm in tissue, and main emission of 27.4-31.4 Kev X-ray and 35.5 Kev γ-ray) were provided by Seeds Biological Pharmacy (Tianjin, China). The ^{125}I seeds were preloaded into the 18-gauge needles and then implanted into the center of left xenografts on mice. The prescribed radiation dose was planned based on the axial micro-CT images using the brachytherapy treatment planning system (Beijing Astro Technology, Beijing, China). Based on measurements of the short (a) and long (b) tumor diameters, tumor volume (TV) and ratio of tumor volume (R_{TV}) were calculated, according to the formula of TV=1/2×a^2×b and R_{TV}=left TV/right TV, respectively.

Micro-PET/CT imaging

^{18}F-FDG was synthesized by the PET/CT Center in our institution. Following an overnight fast, mice were injected with ~0.1 mCi

^{18}F-FDG via the tail vein. After 1 h, mice were anesthetized with 3% isoflurane inhalation and placed in the prone position in the center of a Siemens Inveon combined micro-PET/CT scanner (Siemens Preclinical Solution USA, Inc., Knoxville, TN, USA). Micro-CT scans were performed with an 80 kV X-ray tube voltage, 500 µA current, 150 ms exposure time, and 120 rotation steps. Micro-PET static acquisition was subsequently performed for 10 min and the data were processed using the ordered set expectation maximization algorithm for three-dimensional PET reconstruction. Micro-PET/CT images were analyzed with an Inveon Research Workplace 4.1 (Siemens, Erlangen, Germany). The maximum standardized uptake value (SUVmax; g/ml) of the xenograft was measured before and 28 days after treatment, and the ratio of SUVmax (R_{SUVmax}) was calculated according to the formula of R_{SUVmax}=left SUVmax/right SUVmax.

Immunohistochemistry for caspase-3 expression

All xenografts were fixed in 10% formalin overnight at 4°C and subsequently embedded in paraffin for histological section preparation (4 µm). The sections were deparaffinized and stained with hematoxylin and eosin for normal histological evaluation. IHC was also performed with antibodies to detect caspase-3 expression, according to manufacturer's instructions. The primary antibody (Proteintech Group, Inc., China) used was anti-caspase-3 19677-1-AP (diluted 1: 150). In brief, the sections were immersed in boiled citrate buffer solution (pH 6.0) for 15 min for antigen retrieval after being dewaxed and rehydrated. Then, the sections were bathed 3 times in a phosphate-buffered solution (PBS, pH 7.4) for 3 min each time after being cooled at room temperature, and were quenched in 3% hydrogen peroxide to block endogenous peroxidase activity for 15 min and blocked by normal goat serum for 30 min. Subsequently, the sections were incubated overnight with primary antibody at 4°C and washed 3 times in PBS for 3 min each time. Then, the sections were incubated with horseradish peroxidase-labeled secondary antibodies at 37°C for 20 min and washed 4 times in PBS for 3 min each time, followed by exposure to diaminobenzidine tetrahydrochloride (Dako REAL EnVision Detection System: K5007; Dako, Copenhagen, Denmark). Staining without the primary antibody was performed in parallel and served as a negative control. Finally, the sections were counterstained with hematoxylin, dehydrated in ethanol and xylene, and mounted with cover slips using neutral balsam. Each section was assessed in 3 random fields (×400 magnification) under a BX53 fluorescence microscope (Olympus Co., Tokyo, Japan). The caspase-3 expression of xenograft was semi-quantitively represented as mean optical density (MODcaspase-3) using Image-pro plus software (version 6.0, Media Cybernetics, Inc., Maryland, USA). The ratio of MODcaspase-3 ($R_{MODcaspase-3}$) was obtained according to the formula of $R_{MODcaspase-3}$=left MODcaspase-3/right MODcaspase-3.

TUNEL staining for apoptosis

Tumor cell apoptosis was detected using the In-Situ Cell Death Detection Kit, TMR red (Roche, Basel, Switzerland) with TUNEL technology, in accordance with the manufacturer's instructions. The dewaxed sections were permeabilized with Proteinase K working solution (20µg/ml, provided in the kit) at 37°C for 30 min. After being washed 3 times in PBS for 5 min each time, the sections were incubated with 50 µl of TUNEL reaction mixture (provided in the kit) in a dark and humid atmosphere for 60 min at 37°C and then washed 3 times in PBS for 5 min each time. Subsequently, the sections were incubated in the dark for 5 min with DAPI (Beyotime, Shanghai, China) to stain the nucleus and then washed 4 times in PBST for 5 min each time. Finally, the sections were sealed with anti-fluorescence quenching agent (Southern Biotech, Alabama, USA) and then analyzed under a BX53 fluorescence microscope (Olympus Co., Tokyo, Japan). For quantification of TUNEL-positive cells, the number of TUNEL-positive and total tumor cells was counted in 3 random fields (×400 magnification). The apoptosis index (AI) was calculated as the ratio of TUNEL-positive to total tumor cells. The ratio of AI (R_{AI}) was calculated on basis of R_{AI}=left AI/right AI.

Statistical analyses

All statistical analyses were performed using SPSS 19.0 software (SPSS, Chicago, USA). The continuous variables are described as means ± standard deviation. The significance of difference was evaluated using the paired-samples t test and one-way ANOVA. For one-way ANOVA, if the variances were equal, all pairwise comparisons between group means were performed with the least significant difference test; if they were unequal, Dunnett's T3 test was used. Pearson's analysis was used to evaluate the relationships among R_{TV}, R_{SUVmax}, $R_{MODcaspase-3}$, and R_{AI}. A value of P less than 0.05 was considered statistically significant.

Results

^{125}I-IBT inhibits HepG2 xenograft growth

Figure 1 indicates that compared to right controls, the tumor size of left xenografts decreased after treatment in all groups, especially in the 50 and 80 Gy groups. Table 1 shows that the R_{TV} means of the 50 and 80 Gy group were significantly lower than in the 30 Gy group at 28 days after treatment (P<0.01), while no statistical differences were observed between the 50 and 80 Gy groups (P>0.05). The R_{TV} means after treatment were lower than at baseline in the 50 and 80 Gy groups (P<0.05). These findings suggest that ^{125}I-IBT inhibits growth of HepG2 xenografts, especially at a higher radiation dose.
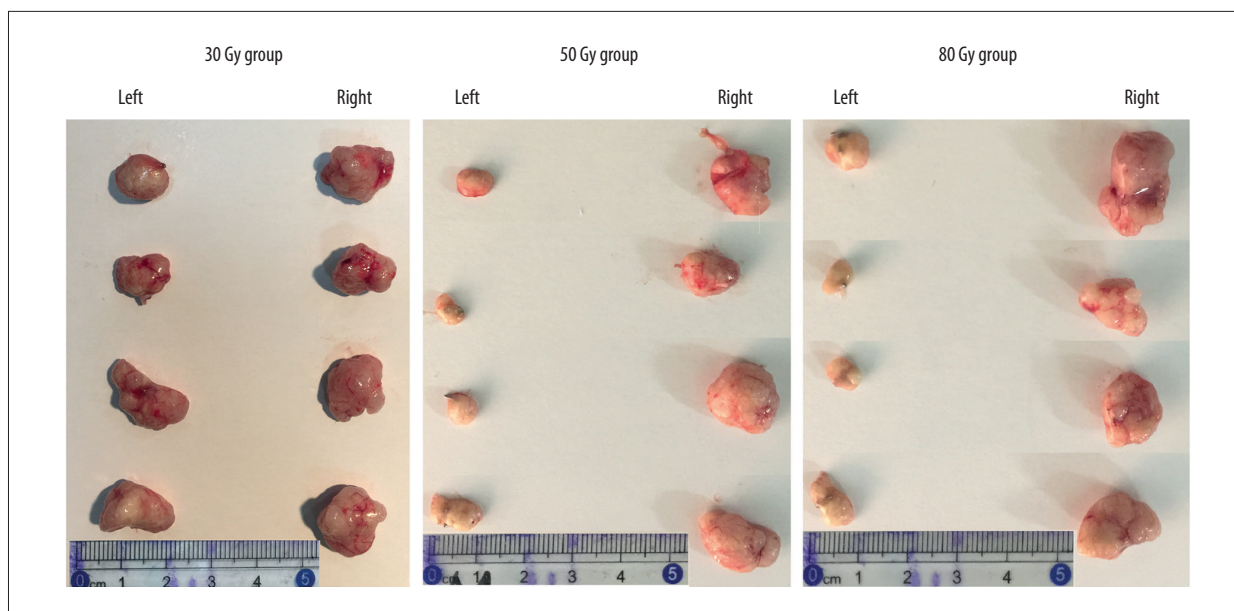
Figure 1. The tumor samples after iodine-125 interstitial brachytherapy (^{125}I-IBT) in hepatocellular carcinoma HepG2 xenografts with a radiation dose of 30, 50, and 80 Gy, respectively. Compared to right controls, the tumor size of left xenografts decreased after ^{125}I-IBT in all groups, especially in 50- and 80-Gy groups.

Table 1. Comparison of tumor volume between before and after ^{125}I-IBT, and among different radiation dose groups in HepG2 xenografts.

Group (n=4)	R_{TV} at baseline	R_{TV} after treatment	t	P value
30 Gy	1.07±0.28	0.59±0.14	2.344	0.1009
50 Gy	1.05±0.44	0.18±0.04*,#	4.185	0.0249
80 Gy	1.07±0.46	0.15±0.08*,#	4.000	0.0280
F	0.005	27.093		
P value	0.9948	0.0002		

^{125}I-IBT – iodine-125 interstitial brachytherapy; R_{TV} – ratio of tumor volume; * $P<0.05$, compared to baseline; # $P<0.01$, compared to 30 Gy group.

^{125}I-IBT reduces ^{18}F-FDG uptake in HepG2 xenografts.

The ^{18}F-FDG uptake patterns in HepG2 xenografts after treatment are shown in Figure 2. The ^{18}F-FDG uptake of left xenografts mildly decreased after treatment in all groups, compared to right controls. The Table 2 showed that the R_{SUVmax} mean after treatment was lower than baseline in 80 Gy group ($P<0.05$), whereas no significant differences were found between them in the 30 and 50 Gy groups ($P<0.05$). The data suggest that ^{125}I-IBT reduces ^{18}F-FDG uptake in HepG2 xenografts, especially at a higher radiation dose.

^{125}I-IBT enhances caspase-3 expression and apoptosis in HepG2 xenografts

The IHC and TUNEL staining patterns of caspase-3 expression and apoptosis in HepG2 xenografts after treatment are shown in Figures 3, 4, respectively. Overall, the caspase-3 expression and tumor cell apoptosis of left xenografts were enhanced after treatment, compared to right controls, and the higher radiation dose had more obvious enhancement. Table 3 shows that the $R_{MODCaspase-3}$ and R_{AI} means of the 80 Gy group were higher than in the 30 Gy group ($P<0.05$), while no significant differences were observed between 50 and 30 Gy, and 80 and 50 Gy groups ($P>0.05$). The data suggest that ^{125}I-IBT upregulates caspase-3 expression and prompts tumor cells apoptosis in HeG2 xenografts, especially at a higher radiation dose.
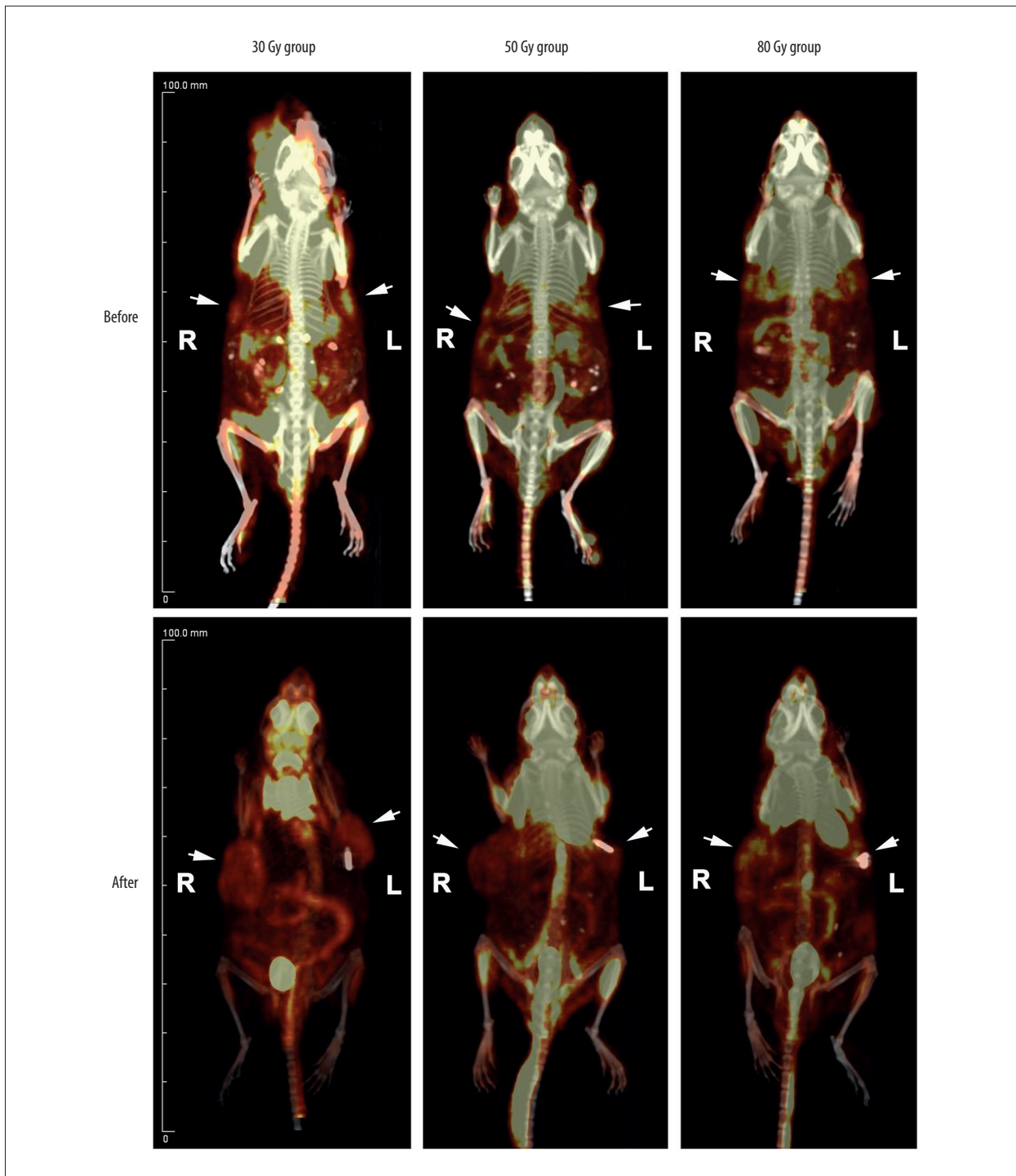
Figure 2. The micro-positron emission tomography/computed tomography with 18F-fluorodeoxyglucose (18F-FDG) in hepatocellular carcinoma HepG2 xenografts before and after iodine-125 interstitial brachytherapy (125I-IBT) with a radiation dose of 30, 50, and 80 Gy, respectively. The maximum intensity projection images showed that the 18F-FDG uptake of left xenografts (arrows) mildly decreased after 125I-IBT in all groups compared to right controls (arrows).

Table 2. Comparison of ^{18}F-FDG uptake between before and after ^{125}I-IBT, and among different radiation dose groups in HepG2 xenografts.

Group (n=4)	R_{SUVmax} at baseline	R_{SUVmax} after treatment	t	P value
30 Gy	0.97±0.16	0.87±0.11	0.979	0.3998
50 Gy	1.02±0.26	0.84±0.08	1.247	0.3009
80 Gy	1.05±0.07	0.78±0.12*	4.740	0.0178
F	0.208	0.876		
P value	0.8158	0.4493		

^{18}F-FDG – ^{18}F-fluorodeoxyglucose; ^{125}I-IBT – iodine-125 interstitial brachytherapy; R_{SUVmax} – ratio of maximum standard uptake value; * P<0.05, compared to baseline.
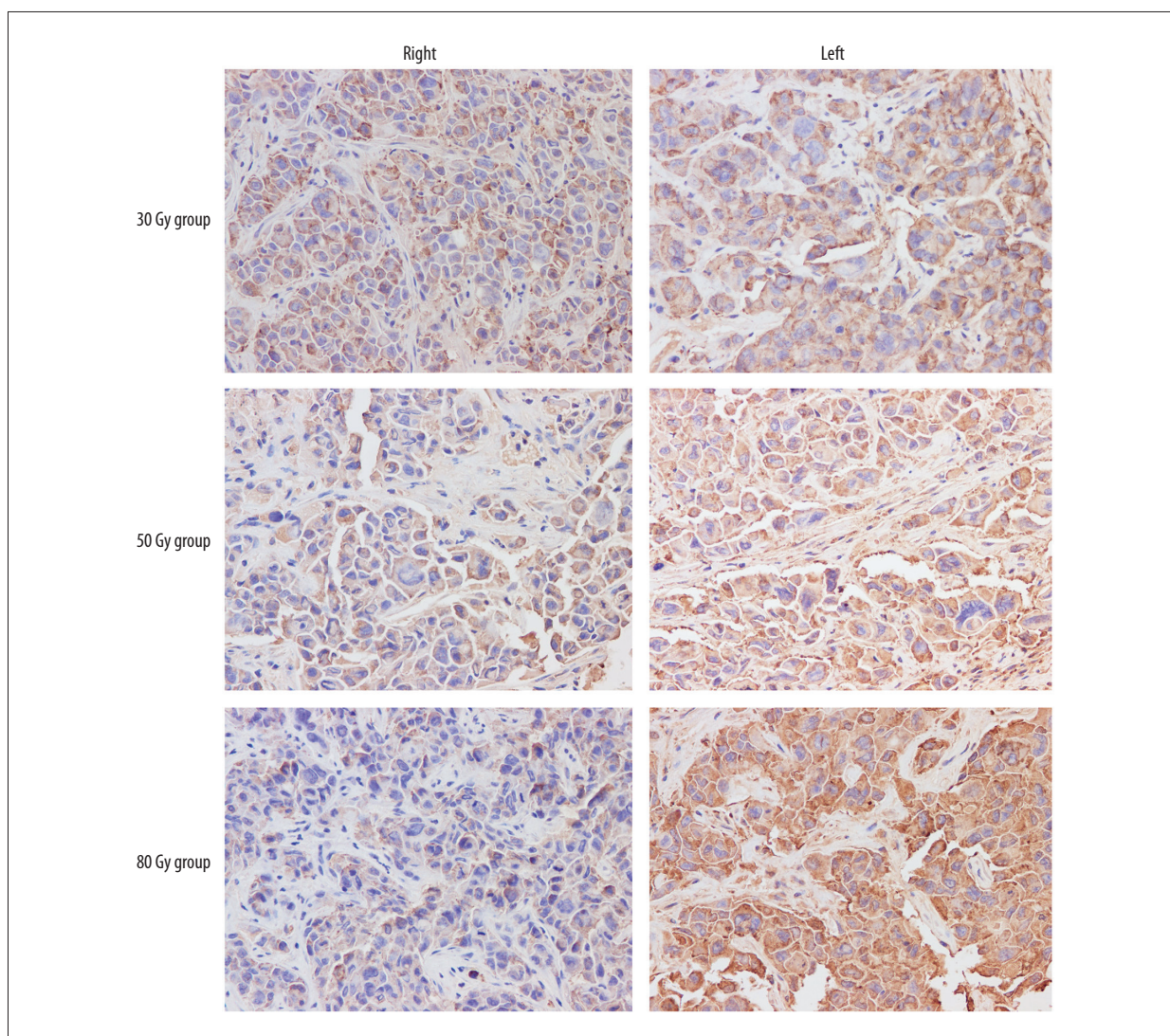

Figure 3. The immunohistochemical (IHC) staining patterns of caspase-3 expression in hepatocellular carcinoma HepG2 xenografts after iodine-125 interstitial brachytherapy (^{125}I-IBT) with a radiation dose of 30, 50, and 80 Gy, respectively (×400). The caspase-3 expression appears brown in IHC staining. These images showed that the caspase-3 expression of left xenografts was upregulated after ^{125}I-IBT compared to right controls, and the higher radiation dose indicated more obvious upregulation.
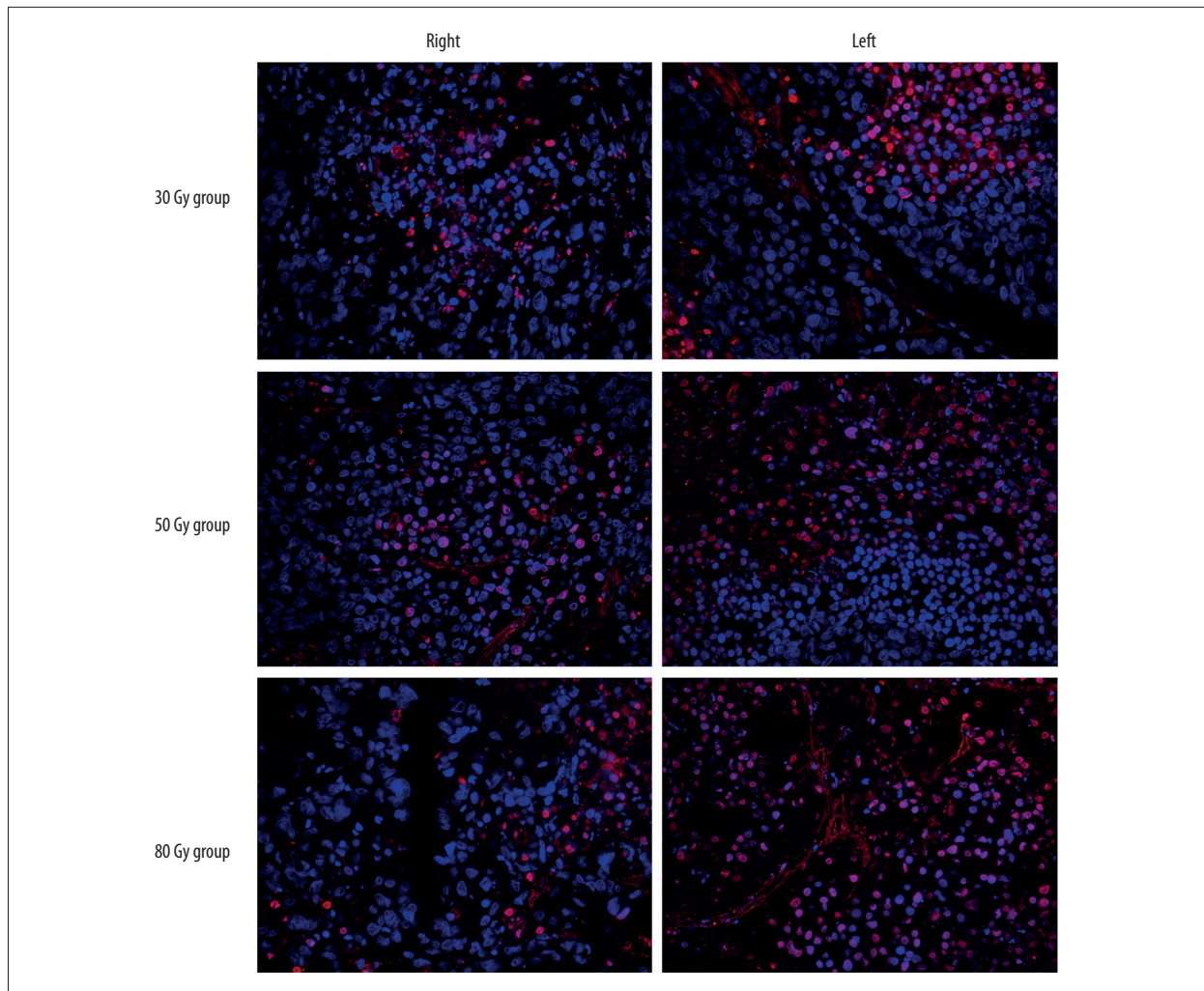
Figure 4. The terminal-deoxynucleotidyl transferase mediated nick-end labeling (TUNEL) staining patterns of apoptosis in hepatocellular carcinoma HepG2 xenografts after iodine-125 interstitial brachytherapy (^{125}I-IBT) with a radiation dose of 30, 50, and 80 Gy, respectively (×400). The apoptotic cells presented red fluorescence in TUNEL staining. These images showed the tumor cell apoptosis of left xenografts was prompted after ^{125}I-IBT compared to right controls, and the higher radiation dose indicated more obvious promotion of apoptosis.

Relationships among ^{18}F-FDG uptake, tumor growth, caspase-3 expression, and apoptosis

The correlations among R_{SUVmax}, R_{TV}, $R_{MODcaspase-3}$, and R_{AI} are shown in Table 4. There was a negative correlation between R_{SUVmax} and $R_{MODcaspase-3}$ (r=−0.624, P<0.05), as well as between R_{SUVmax} and R_{AI} (r=−0.651, P<0.05). Nevertheless, the R_{TV} showed no significant correlation with R_{SUVmax}, $R_{MODcaspase-3}$, and R_{AI}, and $R_{MODcaspase-3}$ was nonsignificantly correlated with R_{AI} (P>0.05).

Discussion

Apoptosis, also known as programmed cell death, is the major mechanism of ionizing radiation-induced cell death. Over the

Table 3. Comparison of caspase-3 expression and apoptosis index among different radiation dose groups after ^{125}I-IBT in HepG2 xenografts.

Group (n=4)	$R_{MODcaspase-3}$	R_{AI}
30 Gy	1.28±0.27	1.45±0.54
50 Gy	1.52±0.34	1.89±0.79
80 Gy	1.83±0.40*	2.85±0.85*
F	2.664	3.76
P value	0.1234	0.0650

^{125}I-IBT – iodine-125 interstitial brachytherapy; $R_{MODcaspase-3}$ – ratio of mean optical density of caspase-3 expression; R_{AI} – ratio of apoptosis index; * P<0.05, compared to 30 Gy group.

Table 4. Relationships among 18F-FDG uptake, tumor growth, caspase-3 expression, and apoptosis in HepG2 xenograft after 125I-IBT.

Correlation coefficient (P value)	R_{TV}	$R_{MODcaspase-3}$	R_{AI}
R_{SUVmax}	0.177　(0.581)	−0.624*　(0.030)	−0.651*　(0.022)
R_{TV}		−0.317　(0.315)	−0.412　(0.183)
$R_{MODcaspase-3}$			0.538　(0.071)

18F-FDG – 18F-fluorodeoxyglucose; 125I-IBT – iodine-125 interstitial brachytherapy; R_{SUVmax} – ratio of maximum standard uptake value; R_{TV} – ratio of tumor volume; $R_{MODcaspase-3}$ – ratio of mean optical density of caspase-3 expression; R_{AI} – ratio of apoptosis index; * P<0.05.

past decade, many preclinical studies have demonstrated that the apoptosis plays key roles in the antitumor activity induced by 125I-IBT, resulting in tumor necrosis and growth inhibition [23–29]. In the present study, tumor growth and apoptosis were evaluated after 125I-IBT with different radiation doses in HCC HepG2 xenografts. Our findings suggest that 125I-IBT prompts tumor apoptosis and inhibits tumor growth in HCC HepG2 xenografts, especially at a higher radiation dose, consistent with the results obtained in previous studies. Ma et al. reported that there were substantially more TUNEL-positive cells in the 125I-IBT group than in the control group, and pancreatic cancer xenograft growth was consequently inhibited [25]. Qin et al. reported that radiation effect was closely associated with radiation dose; as the radiation dose increased, an increase in apoptosis and necrosis was detected in HCC H22 xenografts [30].

Radiation can induce the intrinsic apoptotic pathway (mitochondrial-mediated), the extrinsic apoptotic pathway (death receptor-mediated), or the membrane stress pathway (ceramide production and subsequent second messenger signaling), and then activates the caspase cascade, leading to apoptosis [31]. In the present study, the findings indicated that 125I-IBT upregulated caspase-3 expression in HeG2 xenografts, especially at a higher radiation dose, consistent with a previous report [32]. Caspase-3 protein is the most important executioner protein, and its activation is commonly considered to be the biochemical hallmark of apoptosis. 125I-IBT downregulates epidermal growth factor receptor and vascular endothelial growth factor-A expression, inhibiting protein kinase B (AKT) and extracellular signal regulated kinase (ERK) activation in tumor cells, respectively [26,33]. Moreover, 125I-IBT increases reactive oxygen species (ROS) generation in tumor cells [34]. The inactivated anti-apoptotic AKT and ERK pathways and increasing ROS accelerate the signaling of apoptosis, consequently upregulating caspase-3 expression [31,35].

Aerobic glycolysis, also known as the "Warburg effect", is important for tumor growth and apoptosis. When cancer cells receive an insufficient supply of glucose, cancer metabolism and biomass synthesis slow; cancer cells are then forced to stop growing and then undergo apoptosis [36]. In the present

study, the tumor glucose metabolism was evaluated using 18F-FDG micro-PET/CT imaging after 125I-IBT in HCC HepG2 xenografts, and the relationships among tumor glucose metabolism, growth, and apoptosis were also analyzed. The results showed that 125I-IBT reduces 18F-FDG uptake in HepG2 xenografts, with the largest decrease observed in the 80-Gy group, compared with the baseline, similar to previous results [37]. Jian et al. reported that 18F-FDG uptake in the 125I-IBT group significantly decreased 1 week after treatment, but there was no significant change in controls; this may result from the inactivated AKT and ERK pathways after 125I-IBT mentioned above, which can downregulate glucose transporter-1 expression, resulting in Warburg effect inhibition [38–41]. Moreover, R_{SUVmax} was negatively correlated with $R_{MODcaspase-3}$ and R_{AI} (P<0.05), but there was no significant correlation between R_{TV} and $R_{MODcaspase-3}$ or between R_{TV} and R_{AI} (P>0.05). These findings suggest that 18F-FDG micro-PET/CT may be more useful as a functional imaging modality to assess early response, such as apoptosis, to 125I-IBT in HCC HepG2 xenograft, compared to anatomical size measurement.

Recently, because immunotherapy – especially with immune checkpoint inhibitors such as cytotoxic T lymphocyte-associated antigen 4 (CTLA-4) and programmed cell death 1 (PD-1)/its ligand (PDL-1) blockade, can enhance the systemic antitumor response of radiotherapy (RT) via abscopal effect – the combination of RT and immunotherapy has received extensive attention from oncologists and cancer researchers [42,43]. However, little is known about the efficacy of immune modulation combined with brachytherapy [44,45]. Hodge et al. used carcinoembryonic antigen (CEA)-directed vaccine alone or in combination with 125I-IBT in mice bearing LL2-CEA+ lung adenocarcinoma, and quantified lung metastases, showing that that the combined therapy significantly reduced the burden of metastases in the lungs, demonstrating an abscopal effect [46]. Similarly, Rodriguez-Ruiz et al. used iridium-192 brachytherapy alone or combined with monoclonal antibodies (mAbs) against PD-1 and/or CD137 in mouse models of colorectal cancer to measure the abscopal effect of brachytherapy. Only the combination of brachytherapy and immunostimulatory mAbs resulted in a measurable antitumor response at the nonradiated tumor [47]. These findings provide

promising preclinical evidence supporting use of the combination of brachytherapy and immunotherapy. Further research using ^{18}F-FDG micro-PET/CT imaging is warranted to assess the combination of ^{125}I-IBT and immunotherapy in treating HCC.

In addition, we found no statistically significant difference in levels of $R_{MODcaspase-3}$ and R_{AI} between R_{TV} at baseline and after treatment in the 30-Gy group, as well as between R_{SUVmax} at baseline and after treatment in the 30- and 50-Gy groups and between the 50- and 30-Gy groups. This may have been due to the short study duration of 28 days, as ^{125}I-IBT is typically delivered over a period longer than 180 days [37]. Additionally, 30–50 Gy is a relatively low radiation dose, considering that the clinically effective dose is typically 100–160 Gy [48–51]. Certain limitations of the present study should be considered. First, other key molecules associated with apoptosis were not examined, such as p53, Bax, and Bcl-2. Second, caspase-3 expression was only evaluated using IHC rather than via Western blotting and/or reverse transcription-quantitative polymerase chain reaction assays for transcriptional and translational expression analyses, respectively. Third, the sample size was relatively small and our results cannot be generalized.

Conclusions

The present study suggests that ^{125}I-IBT inhibits tumor growth via upregulating caspase-3 expression and prompting apoptosis in HCC HepG2 xenografts. ^{18}F-FDG micro-PET/CT may be a useful functional imaging modality to assess early response to ^{125}I-IBT in HCC HepG2 xenograft. However, further research on this topic is needed.

Acknowledgements

Conflicts of interest

None.

References:

1. Torre LA, Bray F, Siegel RL et al: Global cancer statistics, 2012. Cancer J Clin, 2015; 65: 87–108

2. Okuda K, Ohtsuki T, Obata H et al: Natural history of hepatocellular carcinoma and prognosis in relation to treatment. Study of 850 patients. Cancer, 1985; 56: 918–28

3. Fong Y, Sun RL, Jarnagin W, Blumgart LH: An analysis of 412 cases of hepatocellular carcinoma at a Western center. Ann Surg, 1999; 229: 790–99, 799–800

4. Llovet JM, Bustamante J, Castells A et al: Natural history of untreated non-surgical hepatocellular carcinoma: Rationale for the design and evaluation of therapeutic trials. Hepatology, 1999; 29: 62–67

5. Yeung YP, Lo CM, Liu CL et al: Natural history of untreated nonsurgical hepatocellular carcinoma. Am J Gastroenterol, 2005; 100: 1995–2004

6. Chun YH, Ahn SH, Park JY et al: Clinical characteristics and treatment outcomes of hepatocellular carcinoma with inferior vena cava/heart invasion. Anticancer Res, 2011; 31: 4641–46

7. Siegel RL, Miller KD, Jemal A: Cancer Statistics, 2018. 2018; 68: 7–30

8. Forner A, Llovet JM, Bruix J: Hepatocellular carcinoma. Lancet, 2012; 379: 1245–55

9. Zhang L, Mu W, Hu CF, Huang XQ: Treatment of portal vein tumor thrombus using (1)(2)5Iodine seed implantation brachytherapy. World J Gastroenterol, 2010; 16: 4876–79

10. Luo J, Yan Z, Liu Q et al: Endovascular placement of iodine-125 seed strand and stent combined with chemoembolization for treatment of hepatocellular carcinoma with tumor thrombus in main portal vein. J Vasc Interv Radiol, 2011; 22: 479–89

11. Chuan-Xing L, Xu H, Bao-Shan H et al: Efficacy of therapy for hepatocellular carcinoma with portal vein tumor thrombus: Chemoembolization and stent combined with iodine-125 seed. Cancer Biol Ther, 2011; 12: 865–71

12. Lin ZY, Chen J, Deng XF: Treatment of hepatocellular carcinoma adjacent to large blood vessels using 1.5T MRI-guided percutaneous radiofrequency ablation combined with iodine-125 radioactive seed implantation. Eur J Radiol, 2012; 81: 3079–83

13. Yang M, Fang Z, Yan Z et al: Transarterial chemoembolisation (TACE) combined with endovascular implantation of an iodine-125 seed strand for the treatment of hepatocellular carcinoma with portal vein tumour thrombosis versus TACE alone: A two-arm, randomised clinical trial. J Cancer Res Clin, 2014; 140: 211–19

14. Yang Q, Zhang W, Liu Q et al: TACE combined with implantation of irradiation stent versus TACE combine with bare stent for HCC complicated by IVCTT. Cardiovasc Inter Rad, 2016; 39: 1280–88

15. Yu TZ, Zhang W, Liu QX et al: Endovascular brachytherapy combined with portal vein stenting and transarterial chemoembolization improves overall survival of hepatocellular carcinoma patients with main portal vein tumor thrombus. Oncotarget, 2017; 8: 12108–19

16. Zhang FJ, Li CX, Zhang L et al: Short- to mid-term evaluation of CT-guided 125I brachytherapy on intra-hepatic recurrent tumors and/or extra-hepatic metastases after liver transplantation for hepatocellular carcinoma. Cancer Biol Ther, 2009; 8: 585–90

17. Bruix J, Gores GJ, Mazzaferro V: Hepatocellular carcinoma: Clinical frontiers and perspectives. Gut, 2014; 63: 844–55

18. Subocz E, Halka J, Dziuk M: The role of FDG-PET in Hodgkin lymphoma. Contemp Oncol (Pozn), 2017; 21: 104–14

19. Cremonesi M, Garibaldi C, Timmerman R et al: Interim 18 F-FDG-PET/CT during chemo-radiotherapy in the management of oesophageal cancer patients. A systematic review. Radiother Oncol, 2017; 125: 200–12

20. Abouzied M, Fathala A, Alsugair A et al: Role of fluorodeoxyglucose-positron emission tomography/computed tomography in the evaluation of head and neck carcinoma. World J Nucl Med, 2017; 16: 257–65

21. Sheikhbahaei S, Mena E, Yanamadala A et al: The value of FDG PET/CT in treatment response assessment, follow-up, and surveillance of lung cancer. Am J Roentgenol, 2017; 208: 420–33

22. Kitajima K, Doi H, Kanda T et al: Present and future roles of FDG-PET/CT imaging in the management of lung cancer. Jpn J Radiol, 2016; 34: 387–99

23. Wang J, Wang J, Liao A et al: The direct biologic effects of radioactive 125I seeds on pancreatic cancer cells PANC-1, at continuous low-dose rates. Cancer Biother Radiopharm, 2009; 24: 409–16

24. Zhuang HQ, Wang JJ, Liao AY et al: The biological effect of 125I seed continuous low dose rate irradiation in CL187 cells. J Exp Clin Cancer Res, 2009; 28: 12

25. Ma JX, Jin ZD, Si PR et al: Continuous and low-energy 125I seed irradiation changes DNA methyltransferases expression patterns and inhibits pancreatic cancer tumor growth. J Exp Clin Cancer Res, 2011; 30: 35

26. Liu J, Wang H, Qu A et al: Combined effects of C225 and 125-iodine seed radiation on colorectal cancer cells. Radiat Oncol, 2013; 8: 219

27. Wang H, Li J, Qu A et al: The different biological effects of single, fractionated and continuous low dose rate irradiation on CL187 colorectal cancer cells. Radiat Oncol, 2013; 8: 196

28. Wang ZM, Lu J, Zhang LY et al: Biological effects of low-dose-rate irradiation of pancreatic carcinoma cells in vitro using 125I seeds. World J Gastroenterol, 2015; 21: 2336–42

29. Xiang G, Zhu X, Lin C et al: 125I seed irradiation induces apoptosis and inhibits angiogenesis by decreasing HIF-1α and VEGF expression in lung carcinoma xenografts. Oncology, 2017; 37: 3075–83

30. Qin QH, Huang BS, Tan QX et al: Radiobiological effect induced by different activities of (125)I seed brachytherapy in a hepatocellular carcinoma model. Int J Clin Exp Med, 2014; 7: 5260–67

31. Maier P, Hartmann L, Wenz F et al: Cellular pathways in response to ionizing radiation and their targetability for tumor radiosensitization. Int J Mol Sci, 2016; 17: 102

32. Wang Z, Zhao Z, Lu J et al: A comparison of the biological effects of 125I seeds continuous low-dose-rate radiation and 60Co high-dose-rate gamma radiation on non-small cell lung cancer cells. PLoS One, 2015; 10: e133728

33. Tian Y, Xie Q, Tian Y et al: Radioactive (1)(2)(5)I seed inhibits the cell growth, migration, and invasion of nasopharyngeal carcinoma by triggering DNA damage and inactivating VEGF-A/ERK signaling. PLOS One, 2013; 8: e74038

34. Tian Y, Xie Q, He J et al: Radioactive 125I seeds inhibit cell growth and epithelial-mesenchymal transition in human glioblastoma multiforme via a ROS-mediated signaling pathway. BMC Cancer, 2015; 15: 1

35. Shinomiya N: New concepts in radiation-induced apoptosis: 'premitotic apoptosis' and 'postmitotic apoptosis'. J Cell Mol Med, 2001; 5: 240–53

36. Chen X, Qian Y, Wu S: The Warburg effect: Evolving interpretations of an established concept. Free Radic Biol Med, 2015; 79: 253–63

37. Jian L, Zhongmin W, Kemin C et al: MicroPET-CT evaluation of interstitial brachytherapy in pancreatic carcinoma xenografts. Acta Radiol, 2013; 54: 800–4

38. Thorens B, Mueckler M: Glucose transporters in the 21st century. Am J Physiol Endocrinol Metab, 2010; 298: E141–45

39. Makinoshima H, Takita M, Saruwatari K et al: Signaling through the phosphatidylinositol 3-Kinase (PI3K)/Mammalian target of rapamycin (mTOR) axis is responsible for aerobic glycolysis mediated by glucose transporter in epidermal growth factor receptor (EGFR)-mutated lung adenocarcinoma. J Biol Chem, 2015; 290: 17495–504

40. Upadhyay M, Samal J, Kandpal M et al: The Warburg effect: Insights from the past decade. Pharmacol Ther, 2013; 137: 318–30

41. Dang CV, Kim JW, Gao P, Yustein J: The interplay between MYC and HIF in cancer. Nat Rev Cancer, 2008; 8: 51–56

42. Liu Y, Dong Y, Kong L et al: Abscopal effect of radiotherapy combined with immune checkpoint inhibitors. J Hematol Oncol, 2018; 11: 104

43. Walle T, Martinez MR, Cerwenka A et al: Radiation effects on antitumor immune responses: Current perspectives and challenges. Ther Adv Med Oncol, 2018; 10: 1960357615

44. Patel RB, Baniel CC, Sriramaneni RN et al: Combining brachytherapy and immunotherapy to achieve in situ tumor vaccination: A review of cooperative mechanisms and clinical opportunities. Brachytherapy, 2018 [Epub ahead of print]

45. Chargari C, Van Limbergen E, Mahantshetty U et al: Radiobiology of brachytherapy: The historical view based on linear quadratic model and perspectives for optimization. Cancer Radiother, 2018; 22: 312–18

46. Hodge JW, Sharp HJ, Gameiro SR: Abscopal regression of antigen disparate tumors by antigen cascade after systemic tumor vaccination in combination with local tumor radiation. Cancer Biother Radiopharm, 2012; 27: 12–22

47. Rodriguez-Ruiz ME, Rodriguez I, Barbes B et al: Brachytherapy attains abscopal effects when combined with immunostimulatory monoclonal antibodies. Brachytherapy, 2017; 16: 1246–51

48. Huo X, Wang H, Yang J et al: Effectiveness and safety of CT-guided (125)I seed brachytherapy for postoperative locoregional recurrence in patients with non-small cell lung cancer. Brachytherapy, 2016; 15: 370–80

49. Li W, Dan G, Jiang J et al: Repeated iodine-125 seed implantations combined with external beam radiotherapy for the treatment of locally recurrent or metastatic stage III/IV non-small cell lung cancer: A retrospective study. Radiat Oncol, 2016; 11: 119

50. Yu X, Li J, Zhong X, He J: Combination of Iodine-125 brachytherapy and chemotherapy for locally recurrent stage III non-small cell lung cancer after concurrent chemoradiotherapy. BMC Cancer, 2015; 15: 656

51. Li W, Guan J, Yang L et al: Iodine-125 brachytherapy improved overall survival of patients with inoperable stage III/IV non-small cell lung cancer versus the conventional radiotherapy. Med Oncol, 2015; 32: 395